Journal of Glaciology, Vol. 43, No. 141, 1996

Seismic-reflection evidence for a deep subglacial trough beneath Jakobshavns Isbræ, West Greenland

TED S. CLARKE* AND KEITH ECHELMEYER
Geophysical Institute, University of Alaska, Fairbanks, Alaska 99775-7320, U.S.A.

ABSTRACT. Seismic-reflection methods were used to determine the ice thickness and basal topography of Jakobshavns Isbræ, a large, fast-moving ice stream/outlet glacier in West Greenland. A method of data analysis was developed which involves the pointwise migration of data from a linear seismic array and a single explosive source; the method yields the depth, horizontal position and slope of the basal reflector. A deep U-shaped subglacial trough was found beneath the entire length of the well-defined ice stream. The trough is incised up to 1500 m into bedrock, and its base lies 1200–1500 m below sea level for at least 70 km inland. Center-line ice thickness along most of the channel is about 2500 m, or about 2.5 times that of the surrounding ice sheet. This prominent bedrock trough was not apparent in existing radio-echo-sounding data. Reflection coefficients indicate that much of the basal interface is probably underlain by compacted, non-deforming sediment. The large ice thickness, coupled with relatively steep surface slopes, leads to high basal shear stresses (200–300 kPa) along the ice stream. The large shear stresses and lack of a deformable bed imply that internal deformation plays a dominant role in the dynamics of Jakobshavns Isbræ.

INTRODUCTION

Jakobshavns Isbræ is one of the largest and fastest outlet glaciers draining the Greenland ice sheet. For 70 km inland it has the surface expression of an ice stream (Fig. 1), with heavily crevassed shear margins between the ice stream and the slower-moving ice sheet in which it is embedded. No bedrock is exposed along its margins except near the 10–14 km long floating terminal area. The ice tongue is 600–1100 m thick, floats in a 1000–1500 m deep fjord and is bounded by gneissic walls extending up to 300 m a.s.l.. Speeds of up to 7 km a^{-1} are reached near the terminus of this glacier, leading to a calving flux of approximately 60 Mt d^{-1}. At 75 km inland the ice is still moving 800 m a^{-1}, and the overall surface slope is relatively steep, dropping 1600 m in 100 km (Echelmeyer and Harrison, 1990; Echelmeyer and others, 1991a).

An understanding of the mechanisms behind this fast flow is important because much of the Greenland ice sheet is drained by outlet glaciers of similar surface expression. While there has been considerable investigation of the long, comparatively flat ice streams draining the West Antarctic ice sheet into the Ross Ice Shelf (e.g. Bentley, 1987; Shabtaie and others, 1987; Alley and Whillans, 1991), the unbuttressed ice streams draining into the Amundsen Sea, such as Pine Island and Thwaites Glaciers, are relatively unknown. These latter glaciers and many of the large outlet glaciers of East Antarctica have surface characteristics which resemble those of Jakobshavns Isbræ (McIntyre, 1985). Similarly, model studies of the Laurentide ice sheet show that there may have existed outlet glaciers which flowed from the central ice sheet through the deep fjords to the east; these may have played an important role in the rapid demise of that ice sheet in the past (Denton and Hughes, 1981). Thus, an understanding of the fast-flow mechanism and dynamics of Jakobshavns Isbræ may be helpful in understanding the dynamics of both past and present-day ice streams and ice sheets.

To understand the flow mechanism of Jakobshavns Isbræ, knowledge of its ice thickness, basal topography and temperature distribution is required. Fieldwork and modeling by Iken and others (1993) and Funk and others (1994) give evidence for a 200–400 m thick basal layer of temperate ice overlain by a cold core of ice which has been carried down from the upper drainage basin by the rapid flow. In this paper we describe seismic measurements of ice thickness in the Jakobshavns drainage basin, and provide a comparison with the airborne radar measurements made previously (Gudmandsen, 1970, 1977) by the Technical University of Denmark (TUD). The seismic experiments were conducted in part to provide detailed ice-thickness information needed for the planning of hot-water drilling and associated ice-temperature measurements (Iken and others, 1989; Humphrey and Echelmeyer, 1990).

* Present address: Geophysical and Polar Research Center, University of Wisconsin, 1215 W. Dayton St., Madison, Wisconsin 53706, U.S.A.

https://doi.org/10.3189/S0022143000004081 Published online by Cambridge University Press

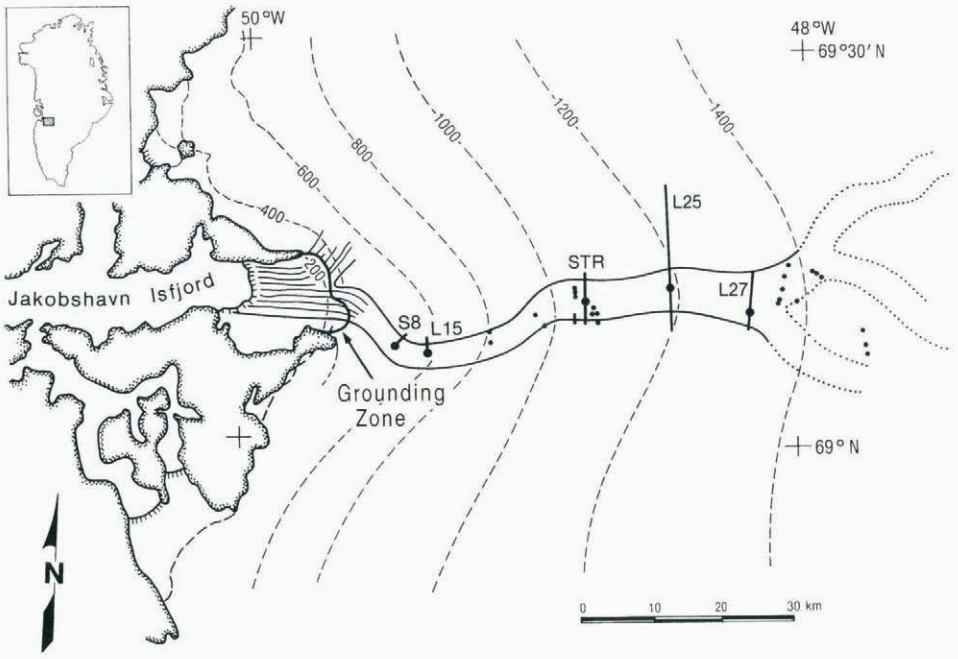

Fig. 1. Location map of Jakobshavns Isbræ. Ice-stream boundaries are shown as solid lines where well defined, dotted in the upper reaches where they are less well defined. Seismic traverses are shown as heavy solid lines with labels that are referred to in the text; small dots represent point seismic measurements, and large dots indicate satellite-derived surface velocity measurement locations described in Echelmeyer and Harrison (1990). Elevation contours in meters are derived from H. Brecher and T. Hughes (personal communication, 1988). Bedrock margins are stippled, and the calving front is shown as a hashed line. Surface elevation and ice-stream boundaries near the grounding zone are approximate.

The method of pointwise migration of seismic-reflection data developed here, to our knowledge, has not been described previously in the glaciological literature. Simple formulae are developed which give depth, horizontal position and slope of the basal reflector from a linear geophone array and a single explosive source. The method has proven useful in other cases where radio-echo sounding has yielded unsatisfactory results due to a large thickness of temperate ice or complex geometry, or both (e.g. Ruth Glacier, Alaska (K. Echelmeyer, unpublished), and Taku Glacier, Alaska (Nolan and others, 1995)).

We first describe the radio-echo-sounding data for the Jakobshavns region which existed prior to our seismic measurements. The seismic methods and analysis are discussed next, followed by a presentation of the seismic results with a synthesis of the radio-echo and seismic data. The measured ice thicknesses are then used to estimate the basal shear stress along the ice stream. Lastly, reflection coefficients are used to investigate the nature of the glacier bed.

RADIO-ECHO SOUNDING OF JAKOBSHAVNS DRAINAGE BASIN

Prior to the joint Eidgenssische Technische Hochschule (ETH) and University of Alaska hot-water drilling program on Jakobshavns Isbræ, a compilation was made of pre-existing data on ice thickness and basal topography in the region. No description of ice thickness of sufficient detail for planning a drilling program had been published. Maps of the entire Greenland ice sheet were presented by Radok and others (1982). Some coarse details of the Jakobshavns drainage basin were tabulated by Bindschadler (1984) using the maps of Radok and others. The source of these ice-thickness data was the airborne radio-echo soundings made by TUD in the 1970s (Overgaard, 1981, 1982, 1984a, b).

The TUD system was a 10 kW ice radar operating at a frequency of 60 MHz . The radar was mounted on an LC-130 aircraft and flown over much of Greenland at altitude of 500–1000 m above the surface. Some of the flights passed over the ocean, sea ice or land, in addition to the ice sheet. Horizontal navigation was done by an inertial navigation system of modest accuracy, and aircraft altitude was determined by pressure altimetry. Z-scope traces were preserved on a photographic film recorder with timing lines (Gudmandsen, 1977).

Because the drilling program required a much more detailed picture of ice-stream thickness than was available from the existing maps, we initiated a search for the actual TUD ice-radar data (Overgaard, 1981, 1982, 1984a, b). Such data were obtained from the World Data Center A — Glaciology (WDCA) in Boulder, Colorado, U.S.A., in the form of tabulations for each flight path over Greenland. The tabulations consisted of latitude, longitude (both to 0.1′), surface elevation and bed elevation at about 1.6 km intervals along parts of each flight. The data were entered into a database, from which contour maps of Jakobshavns drainage basin were constructed. Transverse and longitudinal profiles of ice thickness and surface and bed topography were also constructed. Coverage over the basin was limited, as is shown by the flight paths depicted in Figure 2.

https://doi.org/10.3189/S0022143000004081 Published online by Cambridge University Press

Two features of the radar data are apparent from Figure 2. First, there exist large sections of most flights in this region where no basal returns were identified. Many of the data gaps are over the ice stream or neighboring shear margins; presumably, heavy crevassing caused scattering loss of the radio signals transmitted from the relatively high flying aircraft. Secondly, there were a few crossing points where basal returns were recorded on both profiles. Examination of these crossing points gives an estimate of the errors in the TUD data, both in the positioning system and in the radar itself. We have analyzed the crossing points for which data points from the two flight paths are within 1 km or less of each other. In some cases the bed and surface elevations were interpolated along the intersecting paths to the exact crossing point. The mean difference in elevation of the basal reflector was about 150 m; similar differences existed between the two surface elevations. In addition, some elevations for the ocean surface and the neighboring ice sheet were recorded as 100–200 m below sea. Thus, we take 150–200 m to be a reasonable estimate of the standard error in the elevations and a conservative estimate of the error in ice thicknesses derived from the radar data. A smoothed contour map of ice thickness is shown in Figure 2.

Overlaying the ice-stream boundaries onto the ice thickness map shows no apparent subglacial expression of Jakobshavns ice stream (Fig. 2). This apparent lack of a strong subglacial expression for this ice stream was believed to be similar to what was found beneath some of the West Antarctic ice streams, from both ice radar and seismic measurements (e.g. Shabtaie and others, 1987; Atre and Bentley, 1993; Retzlaff and others, 1993). For planning purposes, an ice depth of 1250 ± 200 m was estimated from Figure 2 for the drill sites near and on the ice stream at about 48.4° W longitude. No depths in excess of 1500 m were expected.

SEISMIC METHODS

Seismic-reflection data were collected during the summers of 1986, 1988, 1989 and 1990. In 1986 a few spot measurements were taken as time allowed between ice-motion surveys. The 1988 season consisted of a single 7 km traverse across the ice stream. The traverse was oriented perpendicular to flow at a location downstream of where the ice stream is clearly defined by intense shear margins. This location was profiled in an effort to determine where the ice stream bed could be reached with the hot-water drilling system. The 1989 season consisted of several partial transverse profiles on the lower ice stream, again in an effort to determine where the base of the ice could be reached by hot-water drilling. The 1990 efforts were aimed at determining the inland extent of the subglacial trough which had been discovered in 1988.

One or two EG&G Geometrics 1210F 12-channel seismographs were used during the various field programs. If two instruments were used, the arrays were occasionally placed at right-angles, with the first geophone of each array at the apex. The two-dimensional array was necessary for depth determinations on the lower ice stream where bottom topography was expected to be somewhat more complicated than that of the inland ice stream, and because the array-shot point arrangements were severely restricted by surface crevassing in the high-strain-rate environment of the lower ice stream. Geophone spacing was 15 m, except in 1990 when 30 m spacing was used. For the spot measurements in 1986, 14 Hz geophones were used; the 1988 and 1990 traverses employed 28 Hz geophones, and both 14 and 28 Hz geophones were used in 1989. The geophones were arranged one per take-out and oriented vertically. The number of samples per channel on the Geometrics receivers is fixed at 1024. All 12 channels were recorded at either 1000 or 2000 samples per second. The resulting

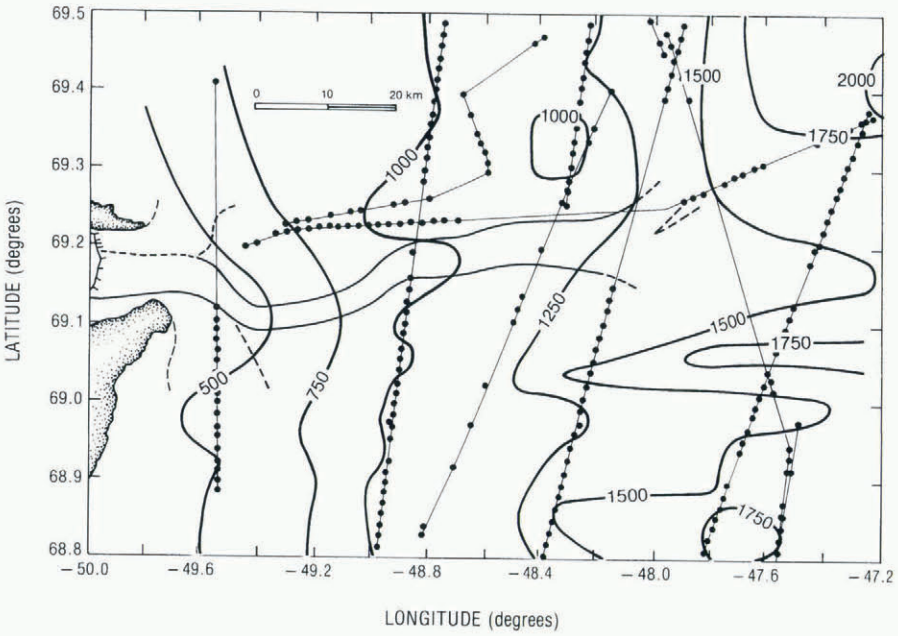

Fig. 2. Map showing TUD ice-radar sounding flight paths and smoothed contours of ice thickness derived from these data, in meters. Dots denote locations where basal returns were recorded. Ice-stream boundaries, calving front and bedrock are shown.

https://doi.org/10.3189/S0022143000004081 Published online by Cambridge University Press

sampling window was rather short and often had to be delayed by up to 1200 ms in order to coincide with the arrival of bottom or wall reflections. In the ablation area, small (0.15–0.5 kg) explosive charges were drilled 2 m into ice; larger charges (up to 2 kg) were placed 3–4 m into the firn of the accumulation area. An analog high-pass filter with a corner frequency of 35–60 Hz was applied to the incoming signal. Data were recorded on paper printouts directly from the seismographs. Examples are shown in Figure 3.

Whenever possible the array was oriented parallel to the dip direction of the reflector. If a single array was employed, this was usually accomplished by first visually estimating bottom topography from surface topography. The array was then oriented perpendicular to the estimated slope of the bed. (We refer to this type of array as a "strike array".) A single shot was then detonated off the immediate end of the array, and deviations from the expected time delay across the array (for a surface-parallel reflector) were used to determine the true strike and dip directions. If the array was not parallel to the strike of the reflector, it was reoriented and another shot was detonated to be sure the strike direction was correct. The final array was then rotated 90° so it would be oriented parallel to true dip in a "dip array". This array orientation was then maintained as the array was moved across the ice stream. The orientation of the dip array was occasionally checked with a strike array and associated shot. This ensured that the depth profile maintained a transverse orientation.

Once the dip array was properly oriented, a shot was detonated either 15 or 30 m from each end of the geophone spread, depending upon geophone spacing along the line of the array. After these initial shots, two different shooting techniques were employed. In 1988 the array and shots were moved across the ice stream one array length at a time, stepwise, after shooting off each end of the array. In 1989 and 1990 the array was left in place while the shot was moved across the ice stream in either direction up to 3 km from the array. After several bed echoes were obtained for a particular array, the array was then relocated 0.5–2 km farther across the ice stream, and several shots were again detonated up- and down-dip from the array. Where bed topography was relatively simple, this shooting technique was found to be expedient in defining the channel shape, because it involved minimum set-up time. Offsets were never large enough to acquire subglacial refractions.

Triggering of the seismograph was accomplished by two methods. The first utilized a thin trigger wire wrapped around the explosive charge. Upon detonation the open circuit of the broken wire triggered the seismograph. While effective and reliable, management of long trigger wires was, at times, difficult. The second method utilized an FM radio trigger system, which, while

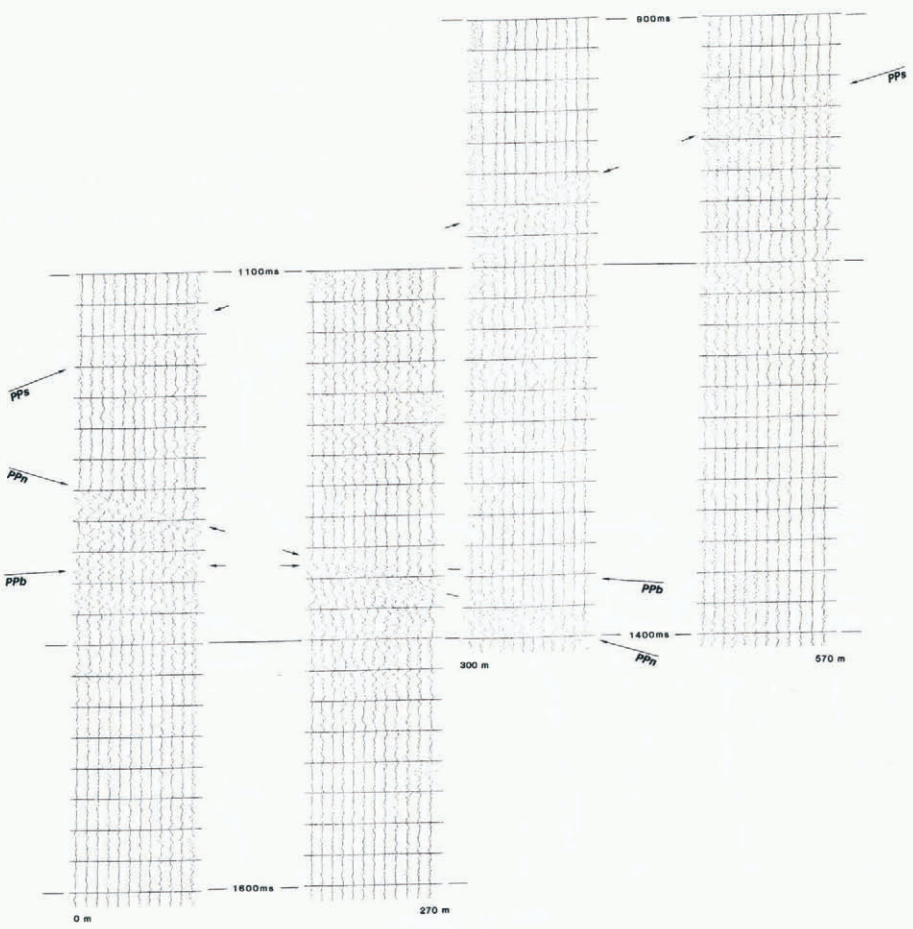

Fig. 3. Sample seismograms from near the center of the STR profile. Several returns are shown, including P-waves reflected from the north and south walls (PP_n, PP_s, respectively) and the P-wave reflection from the center of the trough (PP_b). Timing lines are 25 ms apart. Numbers near the bottom of each seismogram indicate horizontal distance along the surface.

https://doi.org/10.3189/S0022143000004081 Published online by Cambridge University Press

less cumbersome than the trigger wire method, was much more prone to false triggers and failure.

The sample rates usually allowed first arrivals to be determined within 1 ms (about 2 m in depth). In some cases ambiguous returns resulted from high bed roughness, glacier seismic noise, noise resulting from surface wave energy trapped by crevasses, weak echoes, or interfering echoes from different reflectors. The reduced clarity of these echoes increased the error in picking the first arrival to 2 or 3 ms. The worst-case error occurred for two shots on the lowest profile, S8 in Figure 1, where several of these factors combined to create a picking error of about 5 ms (about 10 m in depth).

DATA ANALYSIS

Methods have been developed to ascertain complex basal topography using different types of two-dimensional geophone arrays on a glacier; these have been described by Doell (1963) and Röthlisberger (1972). However, if the geophone spreads can be positioned in a linear array parallel to the dip of the reflecting bed, as we have done, then a simplified formulation for pointwise migration of data from a single shot and a single array can be given. In this section we develop this formulation. Inputs are travel time and shot-to-geophone offset for any two geophones in a dip array. The method yields analytical expressions for the horizontal position, depth and slope of the reflector, assuming a homogeneous isotropic medium over a sloping half-space. The formulation is easily programmed into a pocket electronic calculator which is useful for in-field migration of seismic data and subsequent shot/array location planning.

If the vertical plane defined by the array is perpendicular to the reflecting surface, as for a dip array, then migration becomes a two-dimensional problem. An image point is located equal-distant below the reflector along a bed-perpendicular line (Fig. 4). This distance, h, from the shot point to the image point is given as the solution of

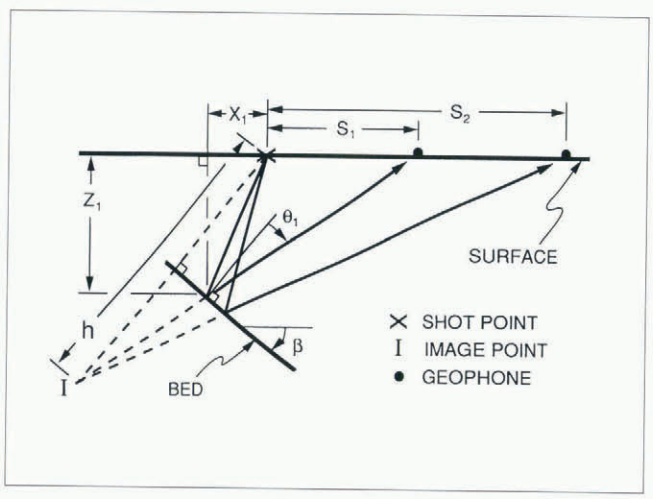

Fig. 4. A sketch of ray-path geometry and image point for a homogeneous isotropic medium overlying a tilted half-space, showing the parameters used in the two-dimensional determination of the reflector location and slope.

$$(v_p t)^2 = s^2 + h^2 - 2hs\cos\left(\frac{\pi}{2} + \beta\right) \qquad (1)$$

where v_p is the P-wave velocity, t is two-way travel time for a given geophone, s is horizontal distance along the surface from the shot to the geophone, and β is the bed slope. A similar equation can be written for a second geophone with the same image point, and the two equations can be solved simultaneously for h:

$$h = \left\{ \frac{s_2\left[(v_p t_1)^2 - s_1^2\right] - s_1\left[(v_p t_2)^2 - s_2^2\right]}{(s_2 - s_1)} \right\}^{\frac{1}{2}}. \qquad (2)$$

Subscripts "1" and "2" designate the two different geophones; they are usually taken to be at the ends of the array. Given h from Equation (2), β can be obtained from Equation (1). The angle of incidence for the ray arriving at geophone 1 is given by

$$\Theta_1 = \cos^{-1}\left\{ \frac{\left[h^2 + (v_p t_1)^2 - s_1^2\right]}{(h v_p t_1)} \right\} \qquad (3)$$

and the vertical ice thickness above the point of reflection, z_1, for the ray arriving at geophone 1 can be determined from

$$z_1 = \frac{h\cos(\beta - \Theta_1)}{2\cos\Theta_1}. \qquad (4)$$

Similarly, the horizontal distance from the shot to the point of reflection, x_1, for the ray arriving at geophone 1 is given by

$$x_1 = -\frac{h\sin(\beta - \Theta_1)}{2\cos\Theta_1}. \qquad (5)$$

With the shot point at the origin, x is positive toward the geophones, and z is positive downward. Equations (4) and (5) assume the array is horizontal. A positive bed slope implies shallower ice under the shot than beneath the geophones; negative β is the reverse. For steep bed slopes the unknown parameters are sensitive functions of the travel-time difference between geophones $(t_1 - t_2)$, and therefore care must be exercised when measuring travel times. The quantities z and x may of course be determined for any geophone in the array if a different s and corresponding time are used. Specifically, if the travel times and distances to the geophones at opposite ends of the array are used separately in Equations (3), (4) and (5), then the end-points of the line segment along the bed which is illuminated by the reflection can be located and plotted.

In our analysis, P-wave velocity was assumed to be that of ice at −15°C: $v_p = 3830\ \mathrm{m\ s^{-1}}$ (Röthlisberger, 1972; Kohnen, 1974). This is based upon the results of Iken and others (1993), who found the ice temperature near site STR (Fig. 1) to vary between about 0°C at the surface, −22°C at 1200 m depth, and melting point again near the base of the ice stream.

Except at the farthest inland seismic locations, shots were drilled directly into ice, and therefore migration of

https://doi.org/10.3189/S0022143000004081 Published online by Cambridge University Press

these data required no firn correction. The geophone spreads were almost always within 1° of horizontal, and never exceeded 4° from horizontal. As discussed previously, the arrays were always oriented as close as possible to the dip direction of the reflector.

The relative positions of the shot points and geophones were determined by optical surveys; they are accurate to about ±2 m. Absolute positions for most arrays were determined by Magnavox Geoceiver satellite Doppler positioning-system methods; they are known to about ±3 m. The absolute locations of the two short traverses on the lower ice stream (S8 and L15 in Figure 1) were determined by air-photo interpretation, and their bearings were determined by compass. These latter arrays have an estimated absolute horizontal accuracy of ±200 m.

SEISMIC DEPTH PROFILES

In this section we present the results of the measurements made along each of the traverses shown in Figure 1. The seismograms shown in Figure 3 illustrate the quality and varying amplitude of the basal reflections. Where possible we compare the seismic results with the TUD airborne radar data.

Description of profiles

In 1988, seismic measurements were made along the profile designated STR (Fig. 1). The stepwise shooting procedure resulted in detailed coverage of most of the bed beneath the transect, with rays of near-normal incidence at all points along the bed. Shot points, and thus the ends of the array, are shown as X's along the surface in Figure 5, where surface and bed topography are displayed with no vertical exaggeration. No basal returns were recorded from the dashed region of the bed profile due to what appears to be a very steep (>50°) transverse bed slope. The profile shows a deep subglacial trough directly beneath the ice stream, with a center-line thickness of 2560 m and a thickness of about 930 m along the margins. The base of the ice stream is approximately 1500 m below sea level at this location. The data shown in Figure 3 were collected from near the center of this profile. Also provided in Figure 5 is a profile of surface velocity, showing the correspondence of ice velocity and ice-stream geometry.

The central borehole shown in Figure 5, drilled in 1988, did not reach the bed owing to the large ice thickness there. The boreholes on the north and south margins of the ice stream were drilled in 1989, after the drilling equipment on the surface had advected downstream about 1 km from the original 1988 profile location. Short seismic profiles were made at each marginal zone beneath these 1989 borehole locations to determine the expected depth for drilling. These results are indicated by the heavy lines and the term "Bed down-glacier" in Figure 5. The boreholes reached the bed at both the north and south margins, and the seismic depths agreed with their actual depths to within ±30 m (2%), thus providing an estimate of the combined errors due to timing,

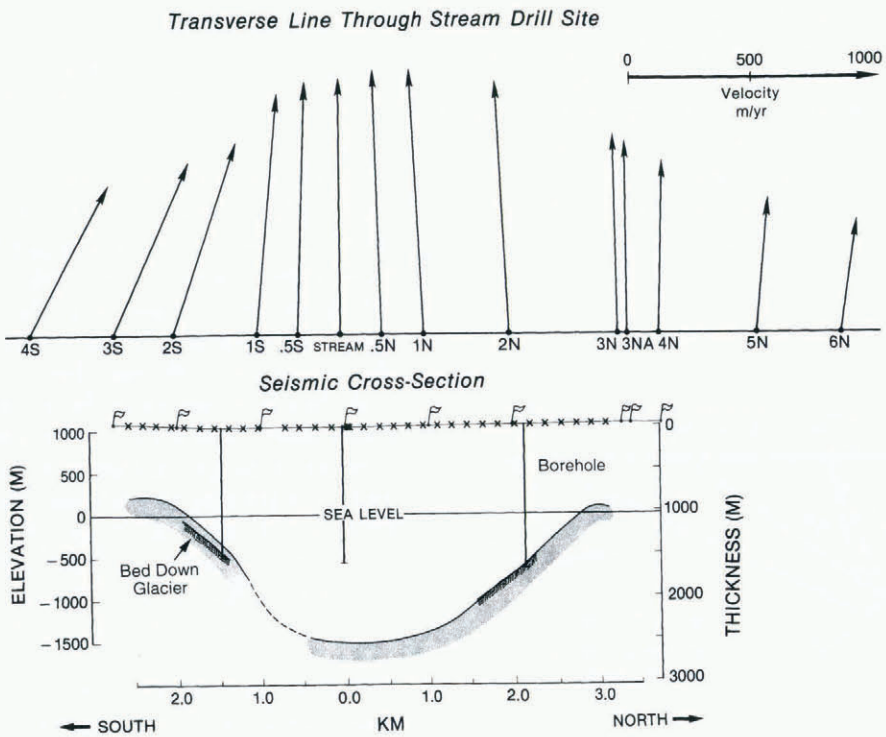

Fig. 5. Lower panel shows the seismically derived cross-section at the STR profile. Shots are shown by X's, and flags represent motion survey poles. The dashed line indicates the area where no basal returns were acquired. Three borehole locations are shown. The two marginal sites were drilled in 1989, after the drilling equipment had advected downstream about 1 km from the STR profile. "Bed down-glacier" refers to reflection data from these two areas. No vertical exaggeration. The upper panel shows annual surface velocity vectors along this transect. Numbers provide distance north and south from the ice-stream center line.

https://doi.org/10.3189/S0022143000004081 Published online by Cambridge University Press

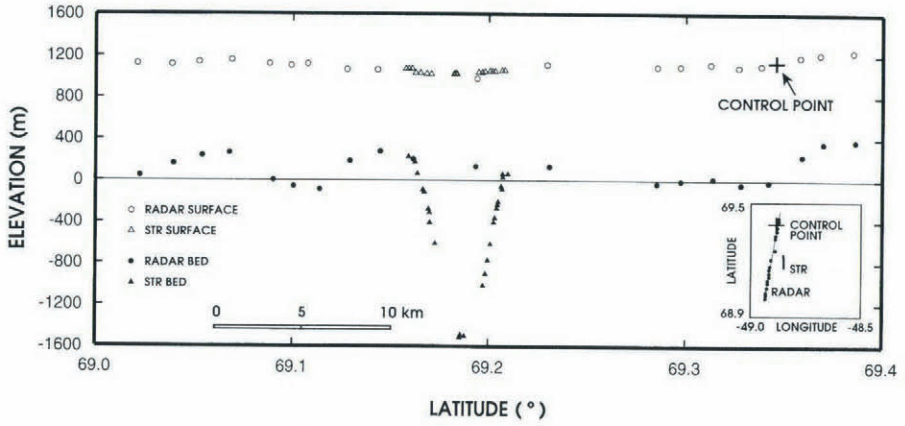

Fig. 6. Comparison of seismic data along STR profile with nearby TUD ice-radar data. The inset shows the location of the radar flight path and the seismic transect. The + marks location of a surface control point surveyed in 1988. Vertical exaggeration is about 6 to 1.

estimated wave speed and migration methods of the survey.

A comparison of this seismic profile with a TUD ice-radar profile is shown in Figure 6. Outside the ice stream the ice thicknesses agree within the error where they can be compared. However, only one radar return is indicated within the boundaries of the ice stream, and this depth is less than half that determined seismically. A Doppler positioning-system control point was surveyed along the radar profile as part of the motion surveys; the TUD surface elevation was found to be about 150 m lower than the control-point elevation and surface elevations at the STR profile. The radar-derived surface and bed elevations were therefore adjusted by this amount.

A 21 km long section was profiled in 1990 at L25, located 12 km upstream from STR (Fig. 1). This profile was acquired both to determine whether the trough was unique to the ice stream, and to determine the influx of ice into the STR profile where the boreholes were drilled. The shear margins of the ice stream were not as intensely crevassed here as they were farther downstream, and yet a trough was found beneath the ice stream which was similar in depth (2580 m) and width to that found at STR (Fig. 7). Ice thickness outside the trough was found to be fairly constant at about 1000 m.

An additional seismic profile was made at L27, about 24 km upstream of STR (Fig. 1). The reflections were of poorer quality, and no reflections were obtained from the channel center line at this location even after several attempts. Shooting near the center of the ice stream at this location resulted in an audible caving sound. These shots were detonated in what was probably a several-meter-thick layer of old lake ice that had been advected downstream from a nearby surface lake, which may partially explain the unusual sounds and lack of returned energy. The estimated basal topography still shows a deep sub-ice-stream trough (Figs 8 and 9a). The estimated center-line ice thickness is about 2800 m, which is greater than that measured anywhere downstream.

Two TUD radar profiles crossed the ice stream between L25 and L27, as indicated in the inset in Figure 8. Considering that the radar flight lines were not as close to the seismic line as those described in Figure 6, we find reasonable agreement between seismic and radar ice thicknesses (within 400 m) outside of the ice stream. However, there is again only one radar reflection indicated over the ice stream itself, and this return shows no subglacial channel.

In 1989, measurements were made at S8, approximately 30 km downstream of STR (Fig. 1), again in preparation for possible drilling there. This location is about 6 km above the grounding zone and has a surface ice speed of about 3800 m a^{-1}. Heavy crevassing in this region placed severe restrictions on the location and mobility of the array there. A right-angle 24-geophone (2 seismograph) array was located near the center of the ice stream, and several shots were detonated up to a few kilometers away with the use of a helicopter. The resulting surface and bed profiles are shown in Figure

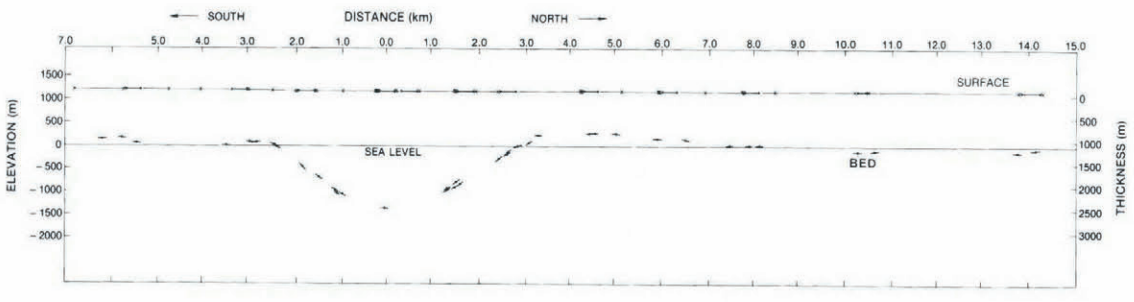

Fig. 7. Seismic profile at L25, with distance from ice-stream center line. Shot points are shown as X's; geophone arrays are short heavy lines along surface; dots with line segments through them indicate a reflection point and associated reflector slope; the length of the associated line segment indicates the section of the bed illuminated by the reflection. No vertical exaggeration. Ice-stream boundaries are located at about 2.6 km south and 3.5 km north of the center line.

https://doi.org/10.3189/S0022143000004081 Published online by Cambridge University Press

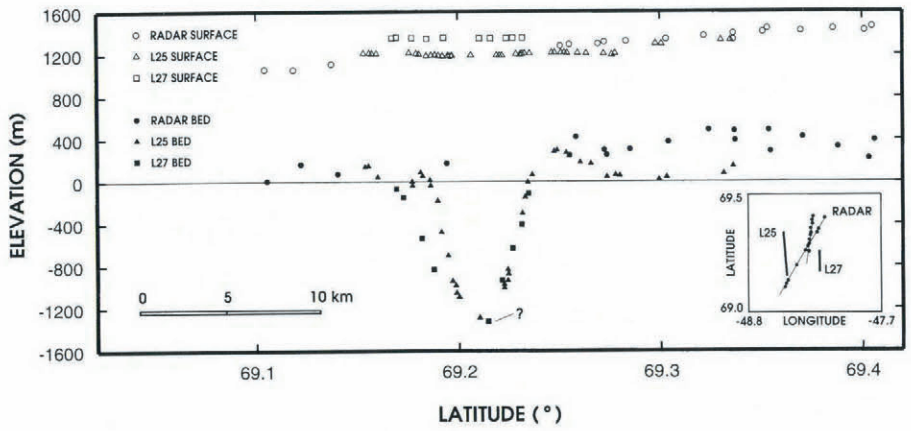

Fig. 8. Comparison of seismic data along the L25 and L27 transects and the TUD ice-radar data along nearby flights. Inset shows location of seismic profiles (heavy lines) and radar flight paths with dots where radar returns were recorded; the two seismic profiles are about 12 km apart. Vertical exaggeration is about 6 to 1.

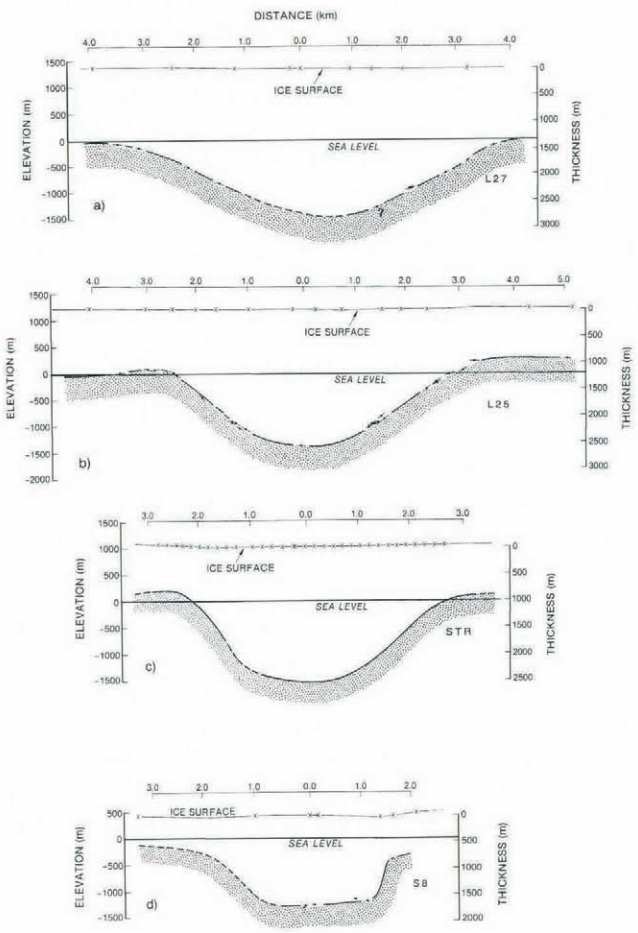

Fig. 9. Four seismic cross-sections of Jakobshavns ice stream from L27 (a) downstream to S8 (d). Shot points are shown as X's; dots with line segments through them indicate a reflection point and associated reflector slope; the length of the associated line segment indicates the section of the bed illuminated by the reflection; dashed lines indicate areas where no reflections were acquired. Ice flow is into the page; north is to the right. All profiles are to the same scale with no vertical exaggeration.

9d. Basal returns are shown as dots, with short lines through them representing the corresponding bed slope. A prominent "transverse" icefall was observed to be flowing sub-perpendicularly into the ice stream about 1.5 km northeast of the array. This icefall overlies the step in the bed which defines the northern margin of the subglacial trough. This basal step was well defined by reflections from the top and bottom of the step, although no returns from the face of the step itself were observed. Center-line thickness was found to be about 1760 m, with a surface elevation of about 500 m. No basal returns were obtained from the southern half of the channel, even after repeated attempts. Thus, the shape of the bed to the south was estimated from the transverse surface morphology of the ice stream at the S8 profile; this estimate is shown by the dashed line there.

Ice thickness distribution

In Figure 9 we plot, to the same scale, the surface and basal topography along each of the profiles described above. From the inland ice at L27 (60 km upstream of the grounding zone) toward S8 (6 km upstream of the grounding zone), the channel narrows markedly, and ice thickness in the center of the stream decreases from about 2800 m to 1760 m. The elevation of the base of the trough increases slightly from about 1500 m to 1260 m below sea level, with an entrenchment into the surrounding bedrock decreasing from 1600 m to 900 m.

The spot seismic measurements made at various locations along the ice stream (Fig. 1) were combined with the profile data to obtain an ice-thickness map of the ice stream as a whole. We have assumed that the ice-radar data are reliable outside the ice stream (which our limited comparisons justify at the ± 200 m level) to produce a contour map of the ice thickness over much of the lower Jakobshavns drainage (Fig. 10).

The ice stream follows the subglacial trough along its length. Two branches of the trough coalesce at about 48° W, and this is mimicked in the surface morphology, although well-defined shear margins are not present at this location. The onset of obvious ice-stream motion begins at roughly the same position as the point of

https://doi.org/10.3189/S0022143000004081 Published online by Cambridge University Press

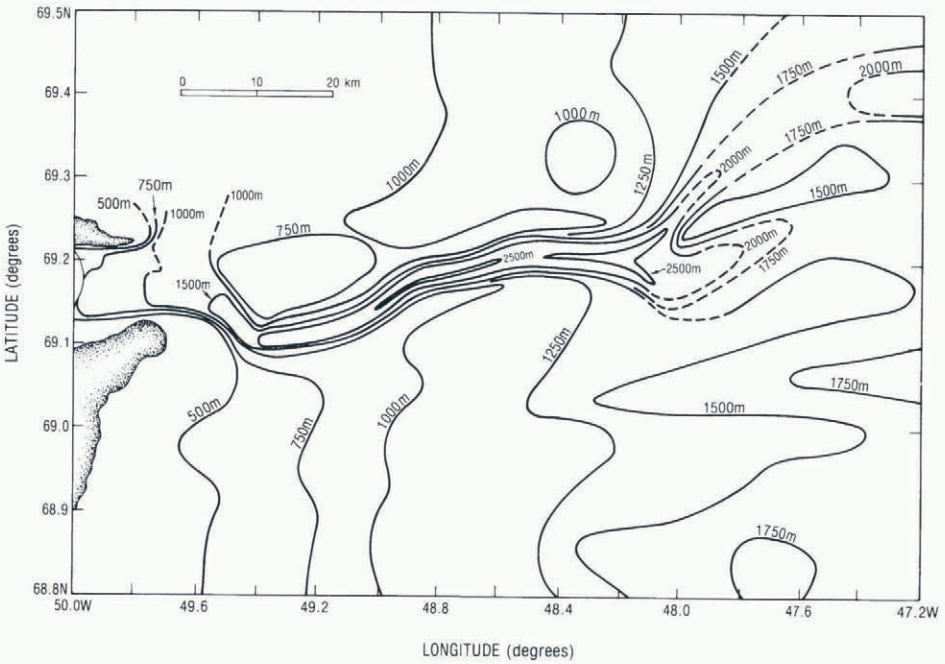

Fig. 10. Map of ice thickness compiled from seismic and TUD ice-radar data. Contours are dashed where poorly constrained.

coalescence. Outside the ice stream, ice thickness is on the order of 900–1400 m, with a gradual thickening toward the interior of the ice sheet. The ice-sheet elevations shown in Figure 1 indicate that the bed of the ice stream is more than 1000 m below sea level along its entire length. No reliable ice-thickness data have been obtained along the northern branch of the ice stream which enters just above the fjord (Fig. 1), but surface morphology, flotation level and speed of this branch indicate that it is not likely to be as thick, nor is a subglacial trough likely to extend very far inland to the north.

BASAL SHEAR STRESS ALONG THE ICE STREAM

The large ice thicknesses along the ice stream, coupled with the relatively steep surface (Echelmeyer and others, 1991a), lead to large basal shear stresses and, consequently, a significant component of ice deformation within the ice stream. The deeply incised bedrock trough and overlying ice complicate the calculation of the basal shear stress, τ_b, within the ice stream. Just as valley walls provide drag along a valley glacier, the walls of the bedrock trough produce drag on the ice stream. In addition, the ice outside the ice stream, which has a different temperature and thickness, provides some drag on the ice stream.

The simple formula $\tau_b = \rho g H \sin\alpha$, where ρ is the density of the ice, g is the acceleration of gravity, H is the ice thickness, and α is the surface slope (where H and α are suitably averaged along the ice stream), must be modified by the incorporation of an effective shape factor, F, which accounts for this wall drag:

$$\tau_b = \rho g F H \sin\alpha \qquad (6)$$

where, now, H is the center-line thickness and $F \in (0, 1]$. F depends on the shape of the trough and the relative stiffness and thickness of ice within the trough and of the ice outside it. The ice alongside the ice stream does provide some drag on the stream as is evidenced by the non-zero transverse shear strain rate observed in the velocity profile at STR (Fig. 5). To account for this additional drag, we make two estimates of an effective shape factor. First, we assume that the ice-sheet surrounding stream is essentially rigid (like the valley walls would be), and then we fit a parabolic shape to the trough and extend it through the overlying ice to the surface (Fig. 11a). The half-width ($W/2$) to center-line ice-thickness (H) ratio for this effective parabolic channel

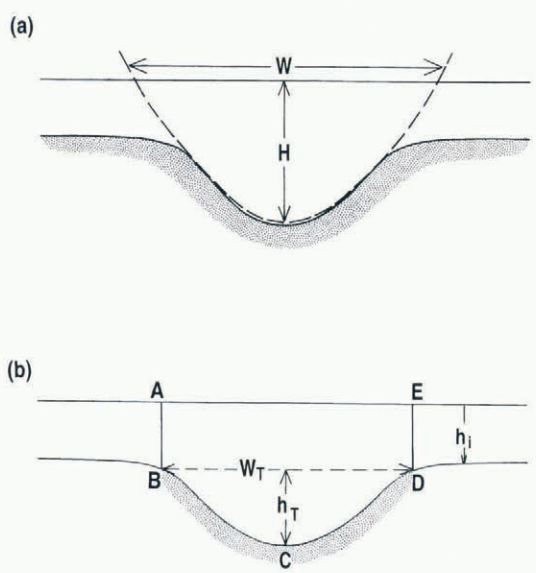

Fig. 11. Sketch showing the geometry assumed in calculating the shape factors. (a) F_1 (b) F_2. Parameters are explained in the text.

https://doi.org/10.3189/S0022143000004081 Published online by Cambridge University Press

can then be used to determine the shape factor, F_1, for each cross-section using the results of Nye (1965). The second method utilizes an intuitive definition of the shape factor:

$$F_2 = \frac{S}{(PH)} \tag{7}$$

where S is the total cross-section area of the channel plus the ice above (ABCDEA, Fig. 11b), and P is the "wetted" perimeter of the channel which provides drag on the ice stream (BCD, Fig 11b). In this case we assume that the ice alongside the ice stream does not produce additional drag on the ice stream. Assuming the trough is parabolic in shape, with depth h_T and width W_T, and denoting the thickness of the overlying ice by h_i (Fig. 11b), we have

$$H = (h_i + h_T) \tag{8}$$

$$S = \left(h_i + \frac{2}{3}h_{T_T}\right)W_T \tag{9}$$

$$P = 2\int_0^{\frac{1}{2}W_T} \sqrt{1 + 4a^2x^2}\,\mathrm{d}x \tag{10}$$

where $a = 4h_T/{W_T}^2$.

F_1 will be a minimum value of the effective shape factor because ice alongside the ice stream is assumed (unrealistically) to be immobile along the parabolic shape, and F_2 is a maximum in that it places all of the drag onto the "wetted" bedrock trough. The values so calculated are given in Table 1, along with basal shear stress calculated from Equation (6) using F_1 and F_2. Surface slope has been estimated from Echelmeyer and others (1991a).

τ_b is uniformly large along the ice stream; it is well in excess of the generally assumed 100 kPa. These large values of τ_b lead to a large component of internal deformation. If we assume that the motion of Jakobshavns Isbræ is entirely due to deformation within the ice stream, then an independent estimate of the basal shear stress, τ_o, can be obtained from the center-line surface velocity, u_o, using the formula

$$\tau_o = \left[\frac{2u_o}{(\mathbf{A}H)}\right]^{\frac{1}{3}} \tag{11}$$

where $\mathbf{A}$ is the flow-law parameter, and we have taken the flow-law exponent to be 3.

The value of the flow-law parameter in Equation (11) requires a choice of the mean ice temperature in the cross-section. This value of $\mathbf{A}$ is best determined by a weighted mean over the center-line ice thickness, with the weighting factor determined by the rate of deformation at each depth. This is because Equation (11) relies on the assumptions that $\dot{\varepsilon} \approx (\mathrm{d}u/2\mathrm{d}y) \approx \mathbf{A}\tau^3$, and $\tau \approx \rho g F y \sin\alpha$, where $\dot{\varepsilon}$ is the vertical shear strain rate, τ is the shear stress and y is taken vertically downward. The appropriate weighted mean of $\mathbf{A}$ can be shown to be

$$\langle \mathbf{A} \rangle = \frac{4}{H^4}\int_0^H \mathbf{A}(y)y^3\mathrm{d}y\,. \tag{12}$$

Using the ice temperature given by Iken and others (1993) and the values of $\mathbf{A}$ as a function of temperature given by Paterson (1981), we find that $\langle \mathbf{A} \rangle = 9 \times 10^{-8}$ kPa^{-3} a^{-1}, corresponding to a deformationally weighted mean temperature of –3°C for the STR profile; this relatively warm value shows the effect of the 200–400 m thick temperate layer at the base. The mean ice temperature is likely to be colder upstream because the temperate layer will be less well developed there. Similarly, the actual mean temperature within a cross-section may be colder because the temperate layer is observed to be thinner near the sides of the channel. Considering these points, we estimate τ_o for the temperature range –3 to –8°C ($\mathbf{A} = 9.0$ to 2.2×10^{-8} kPa^{-3} a^{-1}). Using the center-line velocity from Echelmeyer and Harrison (1990), Equation (11) gives the τ_o values listed in Table 1.

These values agree well with those evaluated using Equations (6)–(10), except at S8. If τ_o is greater than τ_b, then either basal sliding is important or the assumed temperature is too cold, while if τ_b is greater than or equal to τ_o then basal sliding is not important. Examination of Table 1 shows that basal sliding is probably only important near S8, which is located close to the grounding zone. At and upstream of STR the dominant flow mechanism is internal deformation of the ice under the large driving stresses present. This finding is further supported by the lack of any seasonal variation in speed, such as might be expected if surface meltwater were to influence the amount of basal sliding (Echelmeyer and Harrison, 1990), and by the preliminary finite-element modeling of Echelmeyer and others (1991b), who found that internal deformation is

Table 1. Parameters for calculation of effective shape factors and basal shear stress, as described in text and shown in Figure 11. Range of τ_b is that obtained from F_1 to F_2, and the range in τ_o is that for a weighted mean ice temperature of –3° to –8°C

Location	W km	H km	h_i km	h_T km	W_T km	α	u_o km a^{-1}	F_1	F_2	τ_b kPa	τ_o kPa
L27	10.8	2.80	1.40	1.40	7.1	0.011	0.50	0.64	0.91	178–253	158–251
L25	7.4	2.58	1.00	1.58	5.8	0.016	0.80	0.55	0.68	206–253	190–302
STR	7.0	2.56	0.93	1.63	5.2	0.018	1.05	0.54	0.65	218–264	210–332
S8	3.8	1.76	0.86	0.90	3.4	0.023	3.80	0.48	0.71	175–258	361–578

sufficient to provide for the observed ice motion at the STR profile given the observed geometry there. Numerical calculations using the observed temperature field and actual bedrock topography will further investigate the role of internal deformation.

BASAL REFLECTION COEFFICIENT

Several records showing multiple returns were encountered along the STR traverse, some of which are shown in Figure 3. Even a cursory glance at these seismograms reveals markedly stronger wall reflections than those from the center of the trough. When more than one return occurs on the same seismogram, the echo strengths are easily compared, since difficulties arising from variations in geophone coupling, shot coupling and shot size are eliminated; and because the Geometrics 1210 operates with a fixed gain setting, amplitude can be determined directly from the seismograms. In 1988, shots were never detonated farther than 15 m from the end of the array, which resulted in near perpendicular incidence for all reflections, so complications arising from refractions and S-wave conversions are also eliminated. Before the echoes can be compared quantitatively, however, the amplitudes of each return must be modified to account for spherical divergence, bed reflectivity and geophone directivity.

Corrections

If it is assumed that P-wave attenuation in cold ice is small (Röthlisberger, 1972; Bentley and Kohnen, 1976), and that density and wave speed are constant, then spherical divergence can be accounted for using the relation $A_s \propto A_o/(\Delta t)$, where Δt is the travel time from the source to the receiver, A_o is the amplitude of the original pulse a short time after detonation, and A_s is the amplitude of the wave after travel time Δt. If a reflection occurs along the travel path, the relation becomes $A_s \propto A_o|R|/\Delta t$, where R is the reflection coefficient of the ice/bed contact. For a downward-traveling wave normally incident on the bed,

$$R = \frac{I_U - I_L}{I_U + I_L} \tag{13}$$

where I_U and I_L are the acoustic impedances of the upper and lower media, respectively. (The acoustic impedance of a medium is the product of the compressional wave velocity and the density.) Note that $|R|$ has been used in the relation immediately above Equation (13) because A_s is an inherently positive number, whereas R is not. The vertical component of A_s measured by the geophones, denoted A_v, is given approximately by $A_v = A_s \cos\alpha$, where α is the angle of incidence of the ray at the surface. Although not strictly correct, the use of $\cos\alpha$ is a good approximation for rays intersecting the surface at angles of less than 50° from vertical, as is shown in the Appendix. For a given shot, α varies across the array, but, for the geometry under consideration here, this variation is always less than 3°. For the geophone nearest the shot, α is equal to the slope of the interface (within a few tenths of a degree) and, therefore, β from Equations (1) and (2) can be used in place of α. The relationship between the amplitude of the initial pulse and that measured by the geophones then becomes:

$$A_v \propto \frac{A_o|R|}{\Delta t}\cos\beta\,. \tag{14}$$

The quantity A_v is taken to be the maximum amplitude of the return pulse, averaged over 12 channels whenever possible. Mean two-way travel time across the spread is used for Δt.

In Equation (14), both A_o and R are unknown, but for more than one echo on the same record, A_o is common to both and may be eliminated using two different return amplitudes; specifically the amplitude of the wall reflection (subscript "w") and that of the reflection from the center of the trough (subscript "c"):

$$\left|\frac{R_w}{R_c}\right| = \frac{A_{vw}}{A_{vc}}\left(\frac{\Delta t_w}{\Delta t_c}\right)\frac{\cos\beta_c}{\cos\beta_w}\,. \tag{15}$$

The ratio of reflection coefficients, R_w/R_c, is a direct measure of differences in bed type at the two locations. Several such ratios have been calculated from those seismograms acquired along the STR profile which show multiple echoes; the ratios are shown graphically in Figure 12.

From Figure 12 it is clear that the magnitude of the reflection coefficient of the walls is generally about 2–3 times that of the center. The two largest deviations, labeled S1 and N3 in Figure 12, were both caused by a change in

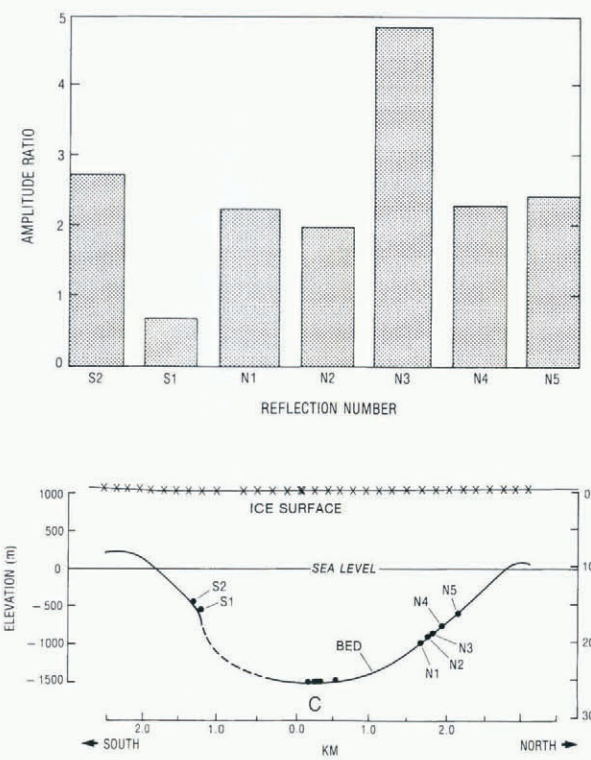

Fig. 12. Upper panel shows several ratios of wall-reflection amplitude to the amplitude of the reflection from the center of the trough. Data are from the STR profile. Lower panel shows the locations of the reflections; C denotes the center of the trough.

https://doi.org/10.3189/S0022143000004081 Published online by Cambridge University Press

echo strength from the wall rather than from the center of the trough. Although the possible explanations for variations in reflection strength are numerous, it may be that a convex and concave bed, respectively, contributed to these deviations. Note that bed slope of the south wall increases from 38° to 53° between the S2 and S1 reflection points (Fig. 12), and is then lost. Also, the reflection causing the large N3 ratio originates in the middle of four other reflection locations on the north wall (Fig. 12), all of which show about half the reflection strength of N3. However, because the sample population is small ($n = 7$), the S1 and N3 ratios cannot be treated as statistical outliers. If they are kept, the mean of the ratios is 2.4; it is 2.3 if they are not. The respective standard deviations are 1.1 and 0.2. We therefore take the possible range of $|R_w/R_c|$ to be 2.4 ± 1.1, but include the possibility that $|R_w/R_c|$ may lie in the more restricted range of 2.3 ± 0.2.

To determine the sign of R_w/R_c, the phases of the reflections must be examined. If one reflection is reversed in phase with respect to the other, R_w/R_c is negative; otherwise it is positive. Unfortunately the signal/noise ratio was such that the first motion for the reflections from the center of the trough could not be accurately determined (Fig. 3). We therefore must carry the possibility that R_w/R_c may be either positive or negative.

Calculation of acoustic impedance

If the acoustic properties of the wall can be estimated, R_w/R_c can be used to investigate the nature of the ice-stream bed. Between 50 km north and 100 km south of the Jakobshavns fjord the exposed bedrock is comprised largely of granodiorite gneiss, and the large-scale structural fabric of southern Greenland trends east–west (Geological Survey of Greenland, 1971). Also, a sample recovered from the bed during the 1989 drilling operation at a location about 1 km downstream of the S2 reflection point was composed of quartz, hornblende, plagioclase and biotite, which is consistent with a granodiorite gneiss source. We therefore make the assumption that the bedrock in the vicinity of STR is comprised of granodiorite gneiss or a similar material, and that the wall echoes are from a relatively clean interface.

Although somewhat variable, 5.0 km s^{-1} and 2.7 Mg m^{-3}, are reasonable estimates of velocity and density, respectively, for granodiorite gneiss (Charmichael, 1982). It is important to note that, because $|R_w/R_c|$ is large, the calculations that follow are not sensitive to the specific rock type assumed. If velocity and density are taken to be 4.0 km s^{-1} and 2.4 Mg m^{-3}, respectively, or 6.0 km s^{-1} and 3.0 Mg m^{-3}, there are no essential changes in the conclusions. The base of the ice stream in the area of the reflections is temperate (Iken and others, 1993), thus the velocity and density of the ice at the interface are taken to be 3.60 km s^{-1} and 0.92 Mg m^{-3}, respectively. From Equation (13) we find $R_w = 0.61$. If $R_w/R_c = 2.4 \pm 1.1$, again using Equation (13), we find that $4.6 \leq I_c \leq$ where I_c is the acoustic impedance of the subglacial material in the center of the trough. If $R_w/R_c = 2.3 \pm 0.2$, $5.3 \leq I_c \leq 6.0$. If R_w/R_c is negative, the two ranges are $1.2 \leq I_c \leq 2.3$ and $1.8 \leq I_c \leq 2.0$, respectively.

The loci of velocity–density pairs which lie in the possible ranges of I_c are shown in Figure 13 as shaded areas. If R_w/R_c is positive, then the most reasonable range for the P-wave velocity of the bed is about 2–4 km s^{-1}, with a corresponding bulk density range of 2.5–2.0 Mg m^{-3}. Within this range lie common velocity–density pairs for lodged tills and other compacted sediments (Charmichael, 1982). The range is further restricted if the S1 and N3 ratios are excluded, but the result is still a compacted sediment. If R_w/R_c is negative, then the material at the bed in the central part of the channel has a velocity and density only slightly greater than that of water, implying that the bed is fluidized.

The bed beneath the central part of the ice stream is more likely to be composed of lodged till or some similar material than to be fluidized, because the results of Echelmeyer and others (1991b), and the close agreement between τ_o and τ_b at this site (Table 1), indicate that basal sliding accounts for, at most, a minor proportion of the surface velocity. However, it is interesting that Iken and others (1993) found that all three of their boreholes on the south side of the ice stream connected to a subglacial drainage system, and in each of them the water level stabilized at about 195 m below the ice surface. The water level required to reduce the effective stress of the ice on its bed to zero under the thick ice in the center of the stream, 1.2 km to the north, is about 212 m below the surface. It is likely from this consideration, and because the slopes of the surface and bed are toward the center of the stream (Shreve, 1972), that the hydraulic gradient also has a component of its slope toward the center of the stream, which would tend to support any existing subglacial water system there. Further, a simple calculation of annual potential energy loss, given W, H, α, and u_o listed in Table 1, and assuming average sectional velocity is $\sim (2/3)u_o$ (Nye, 1965), yields roughly 190 MJ m^{-2} a^{-1} for the ice at site STR. This is equivalent to 0.62 m a^{-1} ice melt. This is a maximum since some energy is absorbed by the cold ice, and all the water produced does not necessarily reach the bed, but it does demonstrate that a fluidized bed is not entirely unreasonable. Weertman (1966) has suggested this as a possible explanation for Jakobshavns' fast flow. It should be noted, however, that the borehole on the north side, which also reached the bed, did not encounter a subglacial drainage system.

For comparison, the estimated density and seismic velocity for the material found beneath a considerable area of Ice Stream B, West Antarctica, are also shown in Figure 13 (Blankenship and others, 1987; Rooney and others, 1987; Kamb and Engelhardt, 1991). These values lie between the two estimates for material beneath Jakobshavns ice stream.

CONCLUSIONS

Seismic-reflection measurements show that a deep subglacial trough underlies Jakobshavns Isbræ for most of its length (Fig. 10). Using the migration method developed here, we find center-line ice thicknesses to be about 2500 m, while the surrounding ice sheet is about 1000 m deep. The ice thicknesses within the stream vary markedly from those shown in Figure 2. Outside the stream, the thicknesses are in agreement with those derived by Fastook and others (1995) but are not in

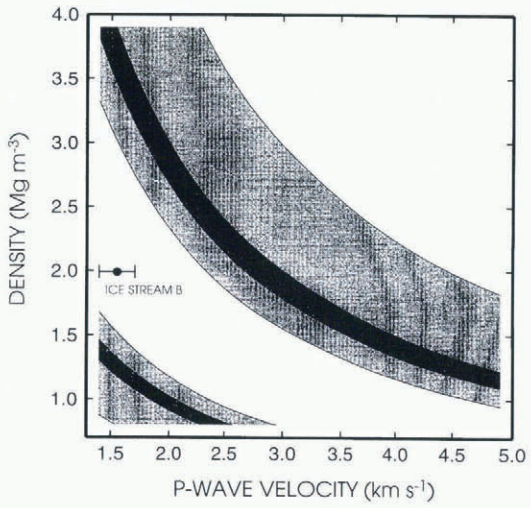

Fig. 13. Diagram of acoustic impedance as contours in the P-wave-velocity, density domain. Shaded regions indicate possible velocity–density pairs for I_c. Light- and dark-gray areas indicate the range of possibilities if $|R_w/R_c| = 2.4 \pm 1.1$ and $|R_w/R_c| = 2.3 \pm 0.2$, respectively. The estimated velocity–density for material beneath Ice Stream B is also shown (Blankenship and others, 1987; Kamb and Engelhardt, 1991).

agreement with those derived within the stream. The onset of obvious ice-stream motion corresponds to the beginning of the main subglacial channel. The bed of the ice stream is more than 1000 m below sea level along most of its length.

Although we have not examined the original records, this subglacial feature was not observed in the radar data available to us. These data show only a few returns over the ice stream, and those present were less than half the seismically derived ice depth. This is due in part to the energy loss at the highly crevassed surface, in part to the absorption loss in the thick ice of the stream, and in part to the broad spread of the wave front after passage through 2000 m of air and ice, which can result in the first reflection coming from the upper edge of the trough. Clearly airborne radio-echo sounding, when flown at an altitude of 500–1000 m above a heavily crevassed surface, must be interpreted with care. Similar conclusions have been reached in Antarctica by C. Swithinbank (personal communication, 1993).

Reflection coefficients indicate that a layer of lodged till or similar sediment is present near the bottom of the trough. Unlike the relatively thin and flat ice streams that drain through the Siple Coast in West Antarctica, a sediment layer need not play a critical role in the dynamics of Jakobshavns Isbræ (Blankenship and others, 1987). This is because the large center-line ice thickness and relatively steep surface slope along the ice stream lead to basal shear stresses on the order of $2.0–2.6 \times 10^5$ kPa. Consequently, we expect rapid internal deformation of the ice. Indeed, the close agreement (Table 1) between the basal shear stress calculated using channel geometry and surface slope, τ_b, and that determined from the center-line surface speed, assuming internal deformation only, τ_o, indicates that internal deformation can account for most of the rapid motion of this ice stream. As expected, sliding or other basal motion contributes more strongly to the speeds observed near the grounding zone (4000–6000 m a^{-1}). A similar flow mechanism has been found to play an important role in the dynamics of Byrd Glacier, Antarctica (Scofield and others, 1991), and may in fact be important in many other ice streams and outlet glaciers draining the Greenland ice sheet, parts of West and East Antarctica, and, possibly, those ice streams which drained the Laurentide ice sheet through deep bedrock channels.

ACKNOWLEDGEMENTS

We wish to thank all those who helped in the fieldwork, including D. Cosgrove, A. Iken, P. Moore, D. Roberts, and especially K. Petersen, and K. Swanson of PICO. We also would like to thank W. Harrison and S. Shabtaie for many helpful comments on the manuscript, and C. Bentley and T. Hughes for their reviews of the manuscript. A. Barrow helped prepare the manuscript.

This work was funded under the U.S. National Science Foundation grant DPP-8722003.

REFERENCES

Aki, K. and P.G. Richards. 1980. *Quantitative seismology. Theory and methods. Vol. 1.* New York, etc., W.H. Freeman and Co.

Alley, R.B. and I.M. Whillans. 1991. Changes in the West Antarctic ice sheet. *Science*, **254**(5034), 959–963.

Atre, S.R. and C.R. Bentley. 1993. Laterally varying basal conditions beneath Ice Streams B and C, West Antarctica. *J. Glaciol.*, **39**(133), 507–514.

Bentley, C.R. 1987. Antarctic ice streams: a review. *J. Geophys. Res.*, **92**(B9), 8843–8858.

Bentley, C.R. and H. Kohnen. 1976. Seismic refraction measurements of internal friction in Antarctic ice. *J. Geophys. Res.*, **81**(8), 1519–1526.

Bindschadler, R.A. 1984. Jakobshavns glacier drainage basin: a balance assessment. *J. Geophys. Res.*, **89**(C2), 2066–2072.

Blankenship, D.D., C.R. Bentley, S.T. Rooney and R.B. Alley. 1987. Till beneath Ice Stream B. 1. Properties derived from seismic travel times. *J. Geophys. Res.*, **92**(B9), 8903–8911.

Charmichael, R.S. 1982. *Handbook of physical properties of rocks. Vol. 2.* Boca Raton, FL, CRC Press.

Denton, G.H. and T.J. Hughes, *eds.* 1981. *The last great ice sheets.* New York, etc., John Wiley and Sons.

Doell, R.R. 1963. Seismic depth study of the Salmon Glacier, British Columbia. *J. Glaciol.*, **4**(34), 425–437.

Echelmeyer, K. and W.D. Harrison. 1990. Jakobshavns Isbræ, West Greenland: seasonal variations in velocity—or lack thereof. *J. Glaciol.*, **36**(122), 82–88.

Echelmeyer, K., R. Wade and A. Iken. 1991a. Mechanisms of ice stream motion: Jakobshavns Isbræ, Greenland. *EOS*, **72**(44), Supplement, 150.

Echelmeyer, K., T.S. Clarke and W.D. Harrison. 1991b. Surficial glaciology of Jakobshavns Isbræ, West Greenland: Part I. Surface morphology. *J. Glaciol.*, **37**(127), 368–382.

Fastook, J.L., H.H. Brecher and T.J. Hughes. 1995. Derived bedrock elevations, strain rates and stresses from measured surface elevations and velocities: Jakobshavns Isbræ, Greenland. *J. Glaciol.*, **41**(137), 161–173.

Funk, M., K. Echelmeyer and A. Iken. 1994. Mechanisms of fast flow in Jakobshavns Isbræ, West Greenland: Part II. Modeling of englacial temperatures. *J. Glaciol.*, **40**(136), 569–585.

Geological Survey of Greenland. 1971. Geologic map of Greenland, Søndre Strømfjord–Nugssuaq sheet, 1:500,000.

Gudmandsen, P.E. 1970. Notes on radar sounding of the Greenland ice sheet. *In* Gudmandsen, P.E., *ed. Proceedings of the International Meeting on Radioglaciology.* Lyngby, Technical University of Denmark. Laboratory of Electromagnetic Theory, 124–135.

Gudmandsen, P. 1977. Studies of ice by means of radio echo sounding. *In* Peel, R.F., *ed. Remote sensing of the terrestrial environment.* London, Butterworths, 198–211.

Humphrey, N. and K. Echelmeyer. 1990. Hot-water drilling and borehole closure in cold ice. *J. Glaciol.*, **36**(124), 287–298.

https://doi.org/10.3189/S0022143000004081 Published online by Cambridge University Press

Iken, A., K. Echelmeyer and W. D. Harrison. 1989. A light-weight hot water drill for large depth: experiences with drilling on Jakobshavns glacier, Greenland. *In* Rado, C. and D. Beaudoing, *eds. Ice core drilling. Proceedings of the Third International Workshop on Ice Drilling Technology, Grenoble–France, 10–14 October 1988.* Grenoble, Laboratoire de Glaciologie et Géophysique de l'Environnement, 123–136.

Iken, A., K. Echelmeyer, W. Harrison and M. Funk. 1993. Mechanisms of fast flow in Jakobshavns Isbræ, West Greenland: Part I. Measurements of temperature and water level in deep boreholes. *J. Glaciol.*, **39**(131), 15–25.

Kamb, B. and H. Engelhardt. 1991. Antarctic Ice Stream B: conditions controlling its motion and interactions with the climate system. *International Association of Hydrological Sciences Publication* 208 (Symposium at St. Petersburg 1990—*Glaciers–Ocean–Atmosphere Interactions*), 145–154.

Kohnen, H. 1974. The temperature dependence of seismic waves in ice. *J. Glaciol.*, **13**(67), 144–147.

McIntyre, N. F. 1985. The dynamics of ice-sheet outlets. *J. Glaciol.*, **31**(108), 99–107.

Nolan, M., R. J. Motkya, K. Echelmeyer and D. C. Trabant. 1995. Ice-thickness measurements of Taku Glacier, Alaska, U.S.A., and their relevance to its recent behavior. *J. Glaciol.*, **41**(139), 541–553.

Nye, J. F. 1965. The flow of a glacier in a channel of rectangular, elliptic or parabolic cross-section. *J. Glaciol.*, **5**(41), 661–690.

Overgaard, S. 1981. *Radio echo soundings in Greenland.* Lyngby, Technical University of Denmark. Electromagnetics Institute. (Data Catalogue 1974.)

Overgaard, S. 1982. *Radio echo soundings in Greenland.* Lyngby, Technical University of Denmark. Electromagnetics Institute. (Data Catalogue 1971/72.)

Overgaard, S. 1984a. *Radio echo soundings in Greenland.* Lyngby, Technical University of Denmark. Electromagnetics Institute. (Data Catalogue 1978.)

Overgaard, S. 1984b. *Radio echo soundings in Greenland.* Lyngby, Technical University of Denmark. Electromagnetics Institute. (Data Catalogue 1979.)

Paterson, W. S. B. 1981. *The physics of glaciers. Second edition.* Oxford, etc., Pergamon Press.

Radok, U., R. G. Barry, D. Jenssen, R. A. Keen, G. N. Kiladis and B. McInnes. 1982. *Climatic and physical characteristics of the Greenland ice sheet.* Boulder, CO, University of Colorado. Cooperative Institute for Research in Environmental Sciences.

Retzlaff, R., N. Lord and C. R. Bentley. 1993. Airborne-radar studies: Ice Streams A, B and C, West Antarctica. *J. Glaciol.*, **39**(133), 495–506.

Rooney, S. T., D. D. Blankenship, R. B. Alley and C. R. Bentley. 1987. Till beneath Ice Stream B. 2. Structure and continuity. *J. Geophys. Res.*, **92**(B9), 8913–8920.

Röthlisberger, H. 1972. Seismic exploration in cold regions. *CRREL Monogr.* II-A2a.

Scofield, J. P., J. L. Fastook and T. J. Hughes. 1991. Evidence for a frozen bed, Byrd Glacier, Antarctica. *J. Geophys. Res.*, **96**(B7), 11,649–11,655.

Shabtaie, S., I. M. Whillans and C. R. Bentley. 1987. The morphology of Ice Streams A, B, and C, West Antarctica, and their environs. *J. Geophys. Res.*, **92**(B9), 8865–8883.

Shreve, R. L. 1972. Movement of water in glaciers. *J. Glaciol.*, **11**(62), 205–214.

Weertman, J. 1966. Effect of a basal water layer on the dimensions of ice sheets. *J. Glaciol.*, **6**(44), 191–207.

APPENDIX

DISCUSSION OF APPROXIMATION IN EQUATION (14)

In estimating acoustic impedance we have assumed that the vertical component of a wave incident on a geophone at the surface can be approximated by a simple cosine function. The validity of using a cosine can be shown as follows. For a non-vertically incident P-wave, the surface displacement is the sum of the displacements caused by the incident P-wave and by P- and S-waves reflected at the free surface. For a plane-wave approximation, the time-harmonic displacement (frequency ω) can be written

$$u_z = [(A_s - A_r)\cos(i) + B_r \sin(r)]e^{-j\omega t} \qquad \text{(A1)}$$

where u_z is the vertical displacement, A_s and A_r are the amplitudes of the incident and reflected P-waves, B_r is the amplitude of the reflected S-wave, i is the angle of incidence and reflection of the P-wave, r is the reflected angle of the S-wave, and $j = \sqrt{-1}$. The ratios of incident to reflected waves at a free surface are

$$\frac{A_r}{A_s} = \frac{\sin(2i)\sin(2r) - \kappa^2 \cos^2(2r)}{\sin(2i)\sin(2r) + \kappa^2 \cos^2(2r)}$$

$$\frac{B_r}{A_s} = \frac{2\kappa \sin(2i)\cos(2r)}{\sin(2i)\sin(2r) + \kappa^2 \cos^2(2r)} \qquad \text{(A2)}$$

where κ is the ratio of v_p to the S-wave speed (Aki and Richards, 1980, sec. 5.2). Combining Equations (A1) and (A2) gives

$$\frac{u_z}{A_s e^{-j\omega t}\cos(i)} = \frac{2\kappa^2}{\kappa^2 \cos(2r) + \sin(2i)\tan(2r)}. \qquad \text{(A3)}$$

The righthand side of Equation (A3) is the factor that our simple cosine correction in Equation (14) ignores. This factor is plotted in Figure 14, where we have assumed that $\kappa = 2.0$ for ice and we have made use of the relation $r = \sin^{-1}[\kappa^{-1}\sin(i)]$. This figure shows that the righthand side of Equation (A3) is essentially constant for $0 < i < 40°$, and thus Equations (14) and (15) are valid approximations over that range. (The factor 2 is a free-surface effect; it cancels out when amplitude ratios are taken.) For $40° < i < 60°$ the error introduced by ignoring this factor is between 1% and 11%. The largest value of i in our study was 53°.

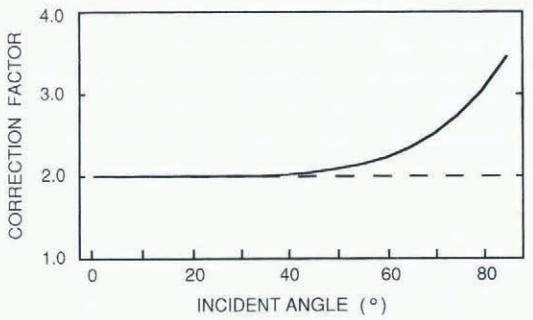

Fig. 14. The correction factor for non-vertical incidence as calculated from the righthand side of Equation (A3).

MS received 10 May 1995 and accepted in revised form 24 October 1995